J. Fluid Mech. (1975), *vol.* 68, *part* 1, *pp.* 1–19
Printed in Great Britain

The role of dynamic pressure in generating fire wind

By R. K. SMITH, B. R. MORTON

Geophysical Fluid Dynamics Laboratory, Monash University, Clayton, Victoria 3168, Australia

AND L. M. LESLIE

Commonwealth Meteorological Research Centre, Melbourne, Victoria 3000, Australia

(Received 29 May 1973 and in revised form 21 February 1974)

Earlier models of fire plumes based on simple entrainment laws and neglecting dynamic pressure have failed to produce the relatively shallow inflow over the fire perimeter known as *fire wind*. This inflow is of prime importance in fire modelling as it normally provides much of the air required for combustion; for this reason we have carried out a very simple numerical experiment on two-dimensional natural convection above a strip heat source with the intention of simulating those aspects of fire behaviour involved in the generation of fire wind without attempting the formidably difficult task of detailed fire modelling. Our results show clearly that fire wind is driven by the dynamic pressure field which is generated by and intimately related to the region of strong buoyant acceleration close above the ground boundary. Throughout our parametric range there is a concentrated region of large horizontal pressure gradient in a neighbourhood above the perimeter of the fire, and elsewhere the pressure gradients play a lesser role.

We have investigated also the dependence of our solution on the boundary conditions, particularly those at the lateral boundary, where we have imposed as little constraint as possible on flow into and out of the computational region. Considerable effects even of such weak side-boundary constraints persist throughout the solution region at moderate values of the pseudo-Rayleigh number (based on eddy diffusivities), but these can be limited by an appropriate choice of the thermal conditions and kept within acceptable bounds at large pseudo-Rayleigh numbers. Similar effects of boundary conditions are likely to appear in other mesoscale convectively driven atmospheric models, including sea breezes, katabatic winds and locally concentrated convective columns.

1. Introduction

Previous attempts to model the air-flow induced by fires have assumed that the convective column (or 'fire plume') produced by a fire rises almost vertically and widens only slowly with height, and that pressure fields play a negligible dynamical role within the column (see, for example, Murgai & Emmons 1960; Lee & Emmons 1961; Nielson & Tao 1965; Morton 1965, 1967; Smith 1969;

Steward 1970). These assumptions have enabled the use of simple plume models, either in direct form, taking temperature variations as relatively small for regions well above the combustion zone, or in modified form to take some account of the much larger changes in temperature near the fire. Such models are valid only within the turbulent fire plume and are broadly consistent with a weak 'entraining' external flow like that of a line sink having strength decreasing with height and centred on the plume axis. This type of approach is based on weak dynamical interaction between the fire plume and its environment and may be satisfactory for fire plumes at appreciable heights above fires of small diameter, but cannot be extended to the neighbourhood of fire sources at the ground. Thus the earlier fire-plume models predict a relatively gentle entrainment at all heights and fail to explain the more concentrated inflow or 'fire wind' which is observed to blow inwards across the perimeter of the fire and which increases in intensity and extent as the fire size and strength increase. This is scarcely surprising as the region within perhaps a source diameter of the ground is one of strong interaction of the buoyant acceleration and the ground boundary, in which the dynamic pressure field must play a role and will produce strong coupling between the fire zone and its environment. It follows that the traditional plume models for fire columns cannot apply near a fire at ground level and should not be expected to predict the observed fire wind; and as the fire wind carries in most of the oxygen required for combustion, such models have serious deficiencies when applied to the combustion zone of a fire.

The great advantage of the earlier models, which apply to slowly spreading fire plumes well above their fire sources, is that asymptotic solutions of a semi-analytic form requiring relatively little computation are available. In the combustion zone and close above it the analytic difficulties are formidable, and even when most of the complications introduced by combustion are ignored there seems to be little chance of obtaining analytic solutions, even to integrated forms of the dynamical equations. In this region it appears probable that solutions will be obtained only by numerical computation over the field of interest, and in this case the problem is further complicated by the need to restrict the solution to a finite computational region, and to choose physically meaningful boundary conditions on the velocity and temperature fields that do not overconstrain the motion above the fire, especially that over the edges of the fire. Our interest is in unconfined fires in the atmosphere, and at least in the simpler cases these are free from lateral boundary constraint. Thus we must select lateral boundary conditions that can be shown to produce little constraint on motion in the fire zone, and yet can be applied within a relatively small distance of the fire so that we are not forced to use an unduly large computational region only sparsely covered with grid points. This is a major problem common to the modelling of a range of mesoscale atmospheric flows, in which the vertical extent of the motion is limited by ambient stratification or by an inversion, and the local flow is produced by buoyancy or other internal forces. It is important in the study of sea breezes and katabatic winds, and also in flows involving concentrated vortices, such as tornadoes, where the force field is due to rotation. Someof our results are relevant in these other flows. They show that overconstraint of motion at the lateral

boundary of flows involving buoyancy can produce significant changes in the motion and temperature fields far from the boundaries, and that the assumption of rigid-wall lateral boundary conditions is acceptable only in cases where it has been demonstrated that the overconstraint is unimportant.

In this paper we describe an attempt to simulate those aspects of fire behaviour involved in the generation of fire wind through a numerical study of two-dimensional natural convection above a horizontal strip source of heat, which forms part of the base of a rectangular computational region large in width and height compared with the half-width of the source. Boundary conditions are chosen to simulate a buoyant upflow of hot air above the source with lateral outflow (or 'venting') under an inversion at a specified height, and with compensating inflow across the lower parts of the side boundary. Such inversions are a common feature of the environment of a large fire; and although a large fire may actually produce some local modification of inversion height, this effect will seldom be big enough during the relatively short duration of the fire to cause significant flow changes near the fire source itself. We have allowed only modest temperature variations, so that we do not attempt to model an actual fire but only to simulate the broad features of strong buoyant acceleration above a horizontal boundary. Thus variations in density are everywhere relatively small, so that their effect is manifest only through the buoyancy forces without changes in fluid mass or inertia per unit volume. Under these conditions, conservation of mass and volume are equivalent to first order, acoustic waves are absent and gravity waves give little trouble because of the fixed inversion height. A simplified form of Navier–Stokes equations can as a result be used, taking reasonable account of the dynamics and allowing for both vertical and horizontal accelerations.

The choice of boundary conditions on the lateral boundary is more critical, as any undue constraint on free inflow of ambient air or outflow of fire-heated air may produce a significant distortion of both the flow field and the dynamic pressure field throughout the computational region. We have assumed zero vertical velocity and local continuity of mass flow; and we have compared the solutions for two thermal conditions: (i) local continuity of heat flux in the outflow and specified ambient temperature in the inflow, and (ii) local continuity of heat flux in both outflow and inflow.

A particular realization of the numerical solution may be characterized by a pseudo-Rayleigh number based on the excess temperature and half-width of the source and on the assumed turbulent diffusivities, and also by the two aspect ratios H/L and H/l, inversion height over width of the computational region and inversion height over source half-width, respectively. In developing the numerical solutions, we shall explore ranges of values of these parameters in order to show that the solution in the neighbourhood of the fire is largely independent of the parameter values provided that they are chosen in suitable ranges.

2. The model

2.1. *The equations of motion*

Consider two-dimensional motion relative to rectangular axes (x, y) with x horizontal and y vertical. The dependent variables include the velocity $\mathbf{u}$, with components (u, v), and the density ρ, temperature T and dynamic pressure p of the air. The equations of motion are, without approximation,

$$\rho D\mathbf{u}/Dt = -\nabla p + (\rho - \rho_0)\,\mathbf{g} + K\rho\nabla^2\mathbf{u}, \tag{1}$$

$$D\rho/Dt = -\rho\nabla.\mathbf{u}, \quad DT/Dt = K\nabla^2 T, \tag{2), (3}$$

where K is a turbulent eddy diffusivity, presumed constant and equal in value for both momentum and heat, $\mathbf{g} = (0, -g)$ is the acceleration due to gravity and t the time.

We assume that the perfect gas law holds and that density changes are associated primarily with temperature changes. Hence the equation of state assumes the simplified form

$$\rho T = \rho_0 T_0, \tag{4}$$

where a subscript zero denotes a constant reference value, being in this case the environmental value at time $t = 0$. We have used potential temperatures and densities to take reasonable account of hydrostatic changes in pressure.

With the Boussinesq approximation, the momentum and continuity equations simplify to

$$\frac{D\mathbf{u}}{Dt} = -\frac{1}{\rho_0}\nabla p - \frac{T - T_0}{T_0}\mathbf{g} + K\nabla^2\mathbf{u} \tag{5}$$

and

$$\nabla.\mathbf{u} = 0, \tag{6}$$

using (4) to express the buoyancy term of (1) in terms of temperature.

Equations (3), (5) and (6) form a closed set and may be used to determine the pressure, temperature and velocity fields given suitable initial and boundary conditions.

2.2. *Initial and boundary conditions*

The heat source is taken along the portion $-l < x < l$ of the level ground $y = 0$ and has a prescribed temperature T_s in excess of the initial ambient temperature T_0 of the fluid, and the maintained outer ground temperature, also T_0. The flow is confined to the region $y > 0$ and is symmetrical about $x = 0$. Accordingly, the computations are performed in the half-region $D = \{(x, y) | 0 < x < L, 0 < y < H\}$ with $l \ll \min(H, L)$, subject to the initial conditions

$$\mathbf{u}(x, y) = 0, \quad T(x, y) = T_0 \quad \text{throughout the region at } t = 0;$$

and the boundary conditions

$$\begin{aligned}
&u(0, y),\ v_x(0, y),\ T_x(0, y) = 0 && \text{on} \quad 0 \leqslant y \leqslant H,\\
&u(x, 0),\ v(x, 0) = 0 && \text{on} \quad 0 \leqslant x \leqslant L,\\
&T(x, 0) = \begin{cases} T_s \\ T_0 \end{cases} && \begin{matrix} \text{on} \quad 0 \leqslant x \leqslant l, \\ \text{on} \quad l \leqslant x \leqslant L, \end{matrix}\\
&\left.\begin{matrix} u(L, y) \leqslant 0, \quad v(L, y) = 0 \\ T(L, y) = T_0 \text{ or } T_x(L, y) = 0 \end{matrix}\right\} && \text{on} \quad 0 \leqslant y < h(t),
\end{aligned}$$

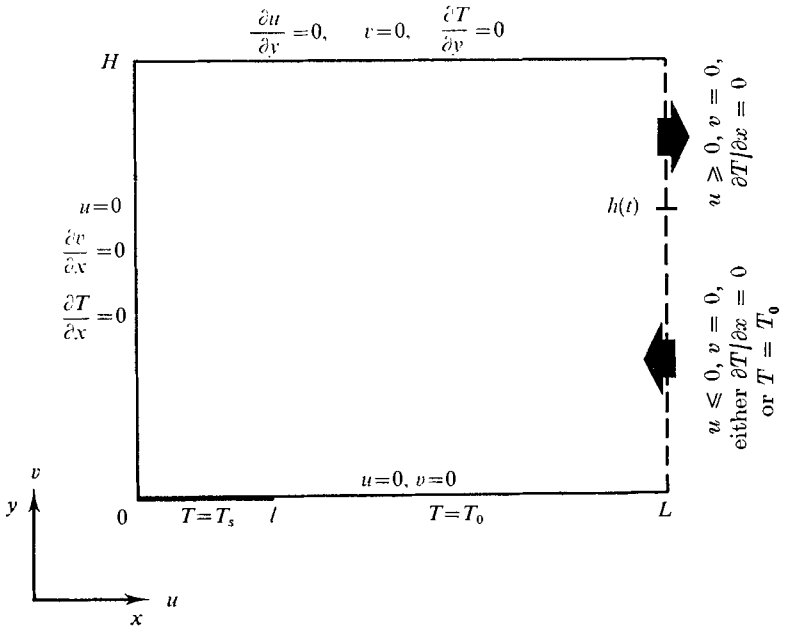

FIGURE 1. Schematic representation of the boundary conditions used in the calculations.

$$u(L,y) \geqslant 0,\ v(L,y),\ T_x(L,y) = 0 \quad \text{on} \quad h(t) \leqslant y \leqslant H,$$

$$u_y(x,H),\ v(x,H),\ T_y(x,H) = 0 \quad \text{on} \quad 0 \leqslant x \leqslant L,$$

where $h(t)$ is determined by the integral constraint

$$\int_0^H u(L,y)\,dy = 0, \tag{7}$$

representing conservation of mass flux (in the Boussinesq approximation) over the lateral boundary as a whole. These conditions are illustrated in figure 1, and are further discussed below.

The conditions on $x = 0$ merely express symmetry. Those on $y = H$ may be thought of as modelling an inversion through which the plume is unable to penetrate; although the assumptions of zero tangential stress and zero heat flux at this level are chosen primarily for mathematical convenience they are consistent with our expectation that there will be insufficient transport of either heat or momentum across the inversion to cause significant effects on the flow near the source in the relatively short duration of most fires. Our assumption that the height of the inversion remains unaffected above the fire will normally be in error, although the effects near the fire due to any local arching of the inversion are likely to be quite small. The selection of lateral boundary conditions at $x = L$ requires care as these must be capable of permitting free inflow and outflow of neutral or stably stratified fluid to and from the computational region. After some preliminary trials, we have found it satisfactory to impose horizontal flow with $v(L,y) = 0$ over the whole height of the open boundary $x = L$; from the continuity equation, this is equivalent to the Neumann condition $\partial u/\partial x = 0$ at

$x = L$ for u. An immediate test of the degree of constraint introduced by requiring that the lateral inflow and outflow be horizontal is provided by the pressure-gradient fields, which for satisfactory lateral boundary conditions should be small in the upper and lower outer corners (where local buoyancy effects are very small). This has proved a convenient test, and has shown that at higher values of the pseudo-Rayleigh number there is little need to relax the constraint of horizontal lateral flow, although at lower pseudo-Rayleigh numbers it may be better to take the inclination of the streamlines constant across the lateral boundary. A gross integral constraint on u is needed since the condition on normal velocity is of Neumann type. This is provided by the requirement of gross mass conservation in the computational region, or in the current approximation conservation of gross volume expressed by (7); this equation can be used at each time step to determine the height $h(t)$ which separates the lower inflow and the upper venting outflow, although a condition on the stream function is simpler to apply numerically (see §3.2).

The condition $T(L, y) = T_0$ for $0 \leqslant y < h(t)$, where $u < 0$, ensures that inflowing air has the temperature of the environment (for either T_0 = constant or $T_0(y)$); and the condition $\partial T(L, y)/\partial x = 0$ for $h(t) \leqslant y \leqslant H$, where $u \geqslant 0$, which in this approximation corresponds to $\partial(\rho c u T)/\partial x = 0$ where c is the appropriate specific heat, ensures continuity of heat flux across the boundary in a locality where heat transport should be dominated by advection (or it may be regarded as ensuring that the thermal stratification of outgoing air is determined by the flow inside D). It is shown in §4 that the alternative condition $\partial T(L, y)/\partial x = 0$ for the inflow zone $0 \leqslant y < h(t)$ causes little change in the flow field at high Rayleigh number when advective transport dominates that due to diffusion, but there may be considerable differences at lower pseudo-Rayleigh numbers when diffusion plays a more significant role.

The flow is naturally driven by buoyancy forces and has no imposed velocity scale; hence the only dynamical parameter of the system is the pseudo-Rayleigh number

$$Ra = g\frac{T_s - T_0}{T_0} l^3 \Big/ K^2,$$

defined in terms of the single eddy diffusivity K. Values of the ordinary Rayleigh number involving molecular diffusivities greatly exceed those of the pseudo-Rayleigh number. The eddy diffusivity K is taken as constant with values in the range 5–100 $\mathrm{m^2\,s^{-1}}$ in our various cases, although our results are presented in terms of the pseudo-Rayleigh number. There are many unsatisfactory features in the use of eddy diffusivities, though we are unable to avoid their use at present, and it is partly for this reason that we have attempted to explore the solutions over a range of Rayleigh numbers.

3. Numerical procedure

3.1. *Finite-difference formulation*

The differential equations (3), (5) and (6) are replaced by finite-difference analogues in a manner similar to that described by Williams (1967) and Quon

(1972). First, the number of dependent variables is reduced by introducing a stream function ψ and the horizontal vorticity component ζ, defined by

$$u = -\partial\psi/\partial y, \quad v = \partial\psi/\partial x$$

and

$$\zeta = \partial v/\partial x - \partial u/\partial y = \nabla^2\psi.$$

The system of equations (3), (5) and (6) reduces after elimination of the pressure to the corresponding system

$$\frac{D\zeta}{Dt} \equiv \frac{\partial\zeta}{\partial t} + J(\psi, \zeta) = \frac{g}{T_0}\frac{\partial T}{\partial x} + K\nabla^2\zeta, \tag{8}$$

$$DT/Dt \equiv \partial T/\partial t + J(\psi, T) = K\nabla^2 T, \tag{9}$$

$$\nabla^2\psi = \zeta, \tag{10}$$

where the convective parts of the total derivatives $D\zeta/Dt$ and DT/Dt have been expressed in Jacobian notation

$$J(\alpha, \beta) \equiv \frac{\partial\alpha}{\partial x}\frac{\partial\beta}{\partial y} - \frac{\partial\alpha}{\partial y}\frac{\partial\beta}{\partial x}.$$

Once ζ, T and ψ have been computed at a time step, the other dependent variables can easily be calculated when required for that time step. The velocity components u and v are obtained as spatial derivatives of the stream function; and ∇p is found directly from the momentum equation (5) when the velocity and temperature fields are known.

The variables ζ, T and ψ are located at the nodes of a uniform mesh in the x, y plane, the co-ordinates of the nodes at any time level $n\Delta t$ ($n = 0, 1, 2, \ldots$) being (ih, jh), where $i = 0, 1, \ldots, I$, $j = 0, 1, \ldots, J$ and h is the grid interval. Using the notation of Lilly (1964) the averaging operator $\overline{\alpha}^x$ and the differencing operator $\delta_x\alpha$ are defined by

$$\overline{\alpha}^x = \tfrac{1}{2}[\alpha(x + \tfrac{1}{2}h) + \alpha(x - \tfrac{1}{2}h)],$$

$$\delta_x\alpha = h^{-1}[\alpha(x + \tfrac{1}{2}h) - \alpha(x - \tfrac{1}{2}h)].$$

In terms of these operators a suitable finite-differencing scheme replacing (8)–(10) is

$$\delta_t\overline{\zeta}^t + J_1(\psi, \zeta) = (g/T_0)\,\delta_x\overline{T}^x + K[\delta_{xx}\zeta + \delta_{yy}\zeta]_{n-1},$$

$$\delta_t\overline{T}^t + J_2(\psi, T) = K[\delta_{xx}T + \delta_{yy}T]_{n-1},$$

$$\delta_{xx}\psi + \delta_{yy}\psi = \zeta,$$

where

$$J_1(\psi, \zeta) = \tfrac{1}{3}[2J_2(\psi, \zeta) + \delta_x\overline{(\psi\delta_y\overline{\zeta}^y)}^x - \delta_y\overline{(\psi\delta_x\overline{\zeta}^x)}^y],$$

$$J_2(\psi, T) = \delta_y(\overline{T}^y\delta_x\overline{\psi}^{xy}) - \delta_x(\overline{T}^x\overline{\psi}^{xy}).$$

The above scheme is centrally differenced in time and uses the Jacobian difference operators devised by Arakawa (1966) to ensure that various integral constraints on the convective terms of the differential equations are preserved in the finite-difference formulation. Finally, the diffusion terms are evaluated at the preceding time level, as indicated by the subscript $n-1$, to prevent computational instability arising from these terms (Platzman 1963).

The numerical procedure consists of successively solving (8)–(10) until the desired state of flow development, usually the steady state, has been reached. The vorticity and temperature finite-difference equations are straightforward evolution equations but the stream-function and vorticity equations comprise a set of simultaneous linear equations for which an accurate method of solution is required, such as the trigonometric interpolation method used by Williams (1967).

3.2. *Initial and boundary conditions*

In terms of the new working variables, the initial conditions become

$$T = \left.\begin{cases} T_s & \text{on} \quad y = 0 \text{ for } 0 \leqslant x \leqslant l \\ T_0 & \text{everywhere else} \end{cases}\right\} \quad \text{at} \quad t = 0. \qquad \zeta, \quad \psi = 0$$

In our calculations we have taken $T_0 = 300\,°\text{K}$ and $T_s = 330\,°\text{K}$. The boundary conditions are now

$$\psi, \zeta, \delta_x T = 0 \quad \text{at} \quad x = 0,$$

$$\psi, \zeta, \delta_y T = 0 \quad \text{at} \quad y = H,$$

$$\psi = 0, \quad T = T_s \quad (0 \leqslant x \leqslant l), \quad T = T_0 \quad (l < x \leqslant L) \quad \text{at} \quad y = 0,$$

and the boundary value of ζ at $y = 0$ is found in a standard way (Williams 1967, p. 149) by applying a one-sided finite-difference approximation to the equation (10) relating the stream function to the vorticity at $y = 0$, and incorporating the no-slip condition into this approximation. At the lateral boundary $x = L$, separate conditions apply in the upper region of outflow and in the lower region of inflow: (i) in the outflow (where $\delta_y \psi < 0$), $\delta_x \psi$, ζ, $\delta_x T = 0$; (ii) in the inflow (where $\delta_y \psi > 0$), $\delta_x \psi = 0$, ζ is calculated from a one-sided (upstream) difference approximation to (10), and *either* $T = T_0$ *or* $\delta_x T = 0$. The gross condition of zero volume flux across the full height of the lateral boundary $x = L$ is obtained from the condition

$$\psi(L, 0) = \psi(L, H)$$

on the stream function $\psi(x, y)$.

3.3. *Stability requirements*

The method described above is computationally stable when subject to the well-known (linear) time-step requirements on the advection and diffusion terms. The Boussinesq approximation filters out acoustic waves and the assumed constant height of the inversion removes the possibility of surface gravity waves. Therefore only internal gravity waves are present. Consequently the necessary condition for computational stability of this flow problem is $\Delta t < \min\left((\Delta x)^2/8\nu, \Delta x/(2U_{\max})^{\frac{1}{2}}\right)$, where the first expression is the diffusive stability requirement and the second, with $U_{\max}$ the maximum velocity in the flow, is the Courant–Friedrichs–Lewy criterion.

Experiment	Ra	H/L ($H/l = \frac{4}{9}8$)	Thermal condition on $x = L,\ y < h$
1	2600	1	$T = T_0$
2		1	$T_x = 0$
3		$\frac{1}{2}$	$T = T_0$
4		$\frac{1}{2}$	$T_x = 0$
5	650	1	$T = T_0$
6		1	$T_x = 0$
7		$\frac{1}{2}$	$T = T_0$
8		$\frac{1}{2}$	$T_x = 0$
9	72	1	$T = T_0$
10		1	$T_x = 0$
11		$\frac{1}{2}$	$T = T_0$
12		$\frac{1}{2}$	$T_x = 0$

TABLE 1

3.4. *Computational requirements*

The calculations were made on an IBM 360/65 computer, where for a 49×49 grid the average time required for a single time step was about 3 s. The most lengthy calculations reached a quasi-steady state after approximately 4000 time steps.

4. Results and discussion

Twelve sets of calculations were performed corresponding to permutations of one of three values of the pseudo-Rayleigh number, one of two values of the aspect ratio H/L (keeping H/l constant) and one of two thermal conditions on inflowing fluid at the lateral boundary. These are summarized in table 1 and will henceforth be referred to by their experiment number. The discussion which follows is based wholly on steady-state flow fields.

Although the calculations were carried out using a 49×49 grid for cases with $H = L$ and a 49×97 grid for $H = 2L$, the solution fields are printed out at every third point on reduced 17×17 and 17×33 grids. The half heat source occupies ten grid points on the lower boundary, and H/l is therefore $\frac{4}{9}8$ in all of the calculations presented. This slightly awkward length ratio had not been intended, but serves as well to display the results as any other.

In natural convection the fluid motion is generated wholly by the gross buoyancy field and consists of ascent of heated fluid and its replacement by cooler ambient fluid. However, buoyancy is strictly a local force which acts to modify the relative position of horizontally adjacent fluid elements at different temperatures or specific weights and is communicated between distant elements of fluid only through the dynamic pressure field; and it is this secondary pressure field that produces both the inflow of almost isothermal ambient air at lower levels and the venting outflow aloft. The customary subdivision into buoyancy and pressure-gradient terms

$$-\frac{1}{\rho_0}\nabla p - \frac{T - T_0}{T_0}\mathbf{g}$$

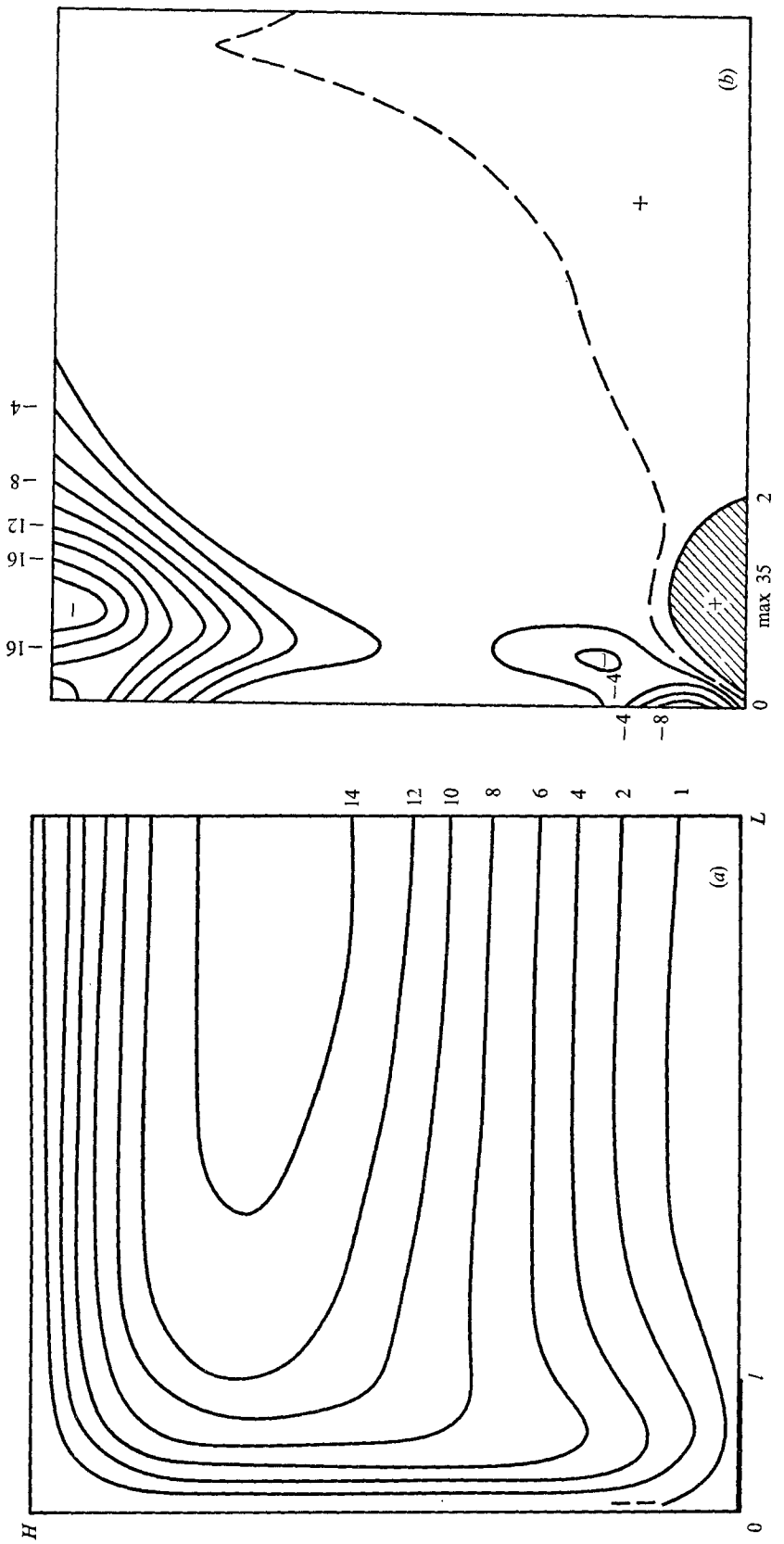
(b)
+
−4
−8
−12
−16
−16
−
+
max 35
2
0
−4
−8
−4
14
12
10
8
6
4
2
1
L
(a)
l
H
0

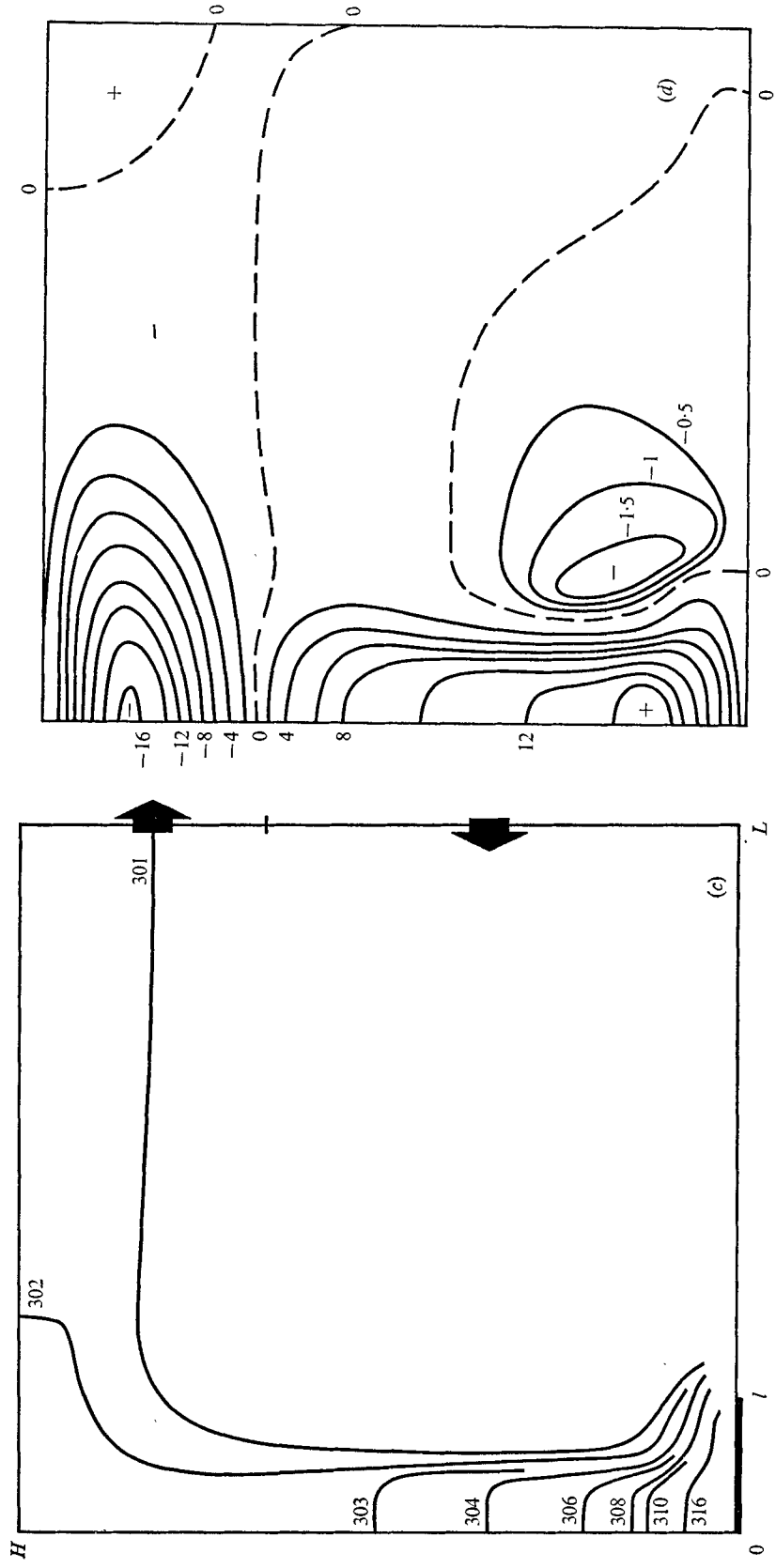

FIGURE 2. Steady-state flow fields including (*a*) streamlines; (*b*) iso-p_x curves; (*c*) isotherms; (*d*) iso-F curves, $F = g(T-T_0)/T_0 - \rho_0^{-1}\partial p/\partial y$; for the prototype calculation with $Ra = 2600$, $H/L = 1$, $H/l = \frac{4\cdot8}{5}$ and with thermal condition $T = T_0$ on the portion $0 \leqslant y < h$ of the lateral boundary $x = L$. Note that, in (*c*), the isotherms are labelled in °K and are *not* equispaced. Only relative values and not absolute magnitudes are ascribed to the streamlines (*a*) and to the iso-p_x (*b*) and iso-F (*d*) curves. Also in (*b*) there is a cell of large positive gradient just above the heat source in which $\rho_0^{-1}p_x$ attains a maximum of approximately 35; contours have not been drawn in this region owing to their close bunching. And in (*d*) the spacing of the closed region of contours just above and to the right of the source perimeter is one-quarter of the spacing elsewhere in this figure.

used in (5) is based on the constant reference temperature T_0 and is purely formal. It is in fact no simple matter to separate the (local) buoyancy and dynamic pressure gradients in the vertical force per unit mass

$$F = g\frac{T-T_0}{T_0} - \frac{1}{\rho_0}\frac{\partial p}{\partial y},$$

and we shall not attempt to do so; however, the horizontal force per unit mass $-\rho_0^{-1}\,\partial p/\partial x$ is pure dynamic pressure gradient.

Figure 2 shows the streamlines, isotherms, contours of the horizontal dynamic pressure gradient (iso-p_x curves) and contours of the vertical force F (iso-F curves) for experiment 1 ($Ra = 2600$, $H/L = 1$, $T = T_0$ on $0 \leqslant y < h$). The flow shows slight retardation above the outer parts of the lower boundary with weak upward tilting of the streamlines followed by a low-level 'sink-like' inflow towards the edges of the fire, a narrow convection column (or 'fire plume') above the source, and a region of venting outflow under the 'inversion' (figure 2*a*). The inflow is nearly isothermal with temperature T_0 (figure 2*c*), showing that, at values of the pseudo-Rayleigh number as high as 2600, heat transfer is dominated by advection in the outer parts of the flow. The pattern of iso-p_x contours (figure 2*b*) shows a region of strong positive gradient centred over the perimeter of the source and roughly one-third of the source width (i.e. $\frac{2}{3}l$) in height. The neighbourhood a little above and to the right of the source perimeter is also a region of moderately strong and negative total force corresponding to the sink-like downflow towards the source (figure 2*d*). These force fields are responsible for driving the concentrated inward and slightly downward 'sink-like' flow above the source perimeter that in our view corresponds to the well-known 'fire wind'.

Above the central regions of the heat source the inflow of air must be deflected upwards into the fire plume, and in this neighbourhood figures 2(*b*) and (*d*) show large negative horizontal pressure gradients and large positive values for the vertical force F. Over the inner parts of the source the isotherms are rather flat at small heights with the result that in this region there is approximate reversed stagnation point flow with little *local* effect of buoyancy, and there must be a mean stagnation point with a pressure maximum at the centre of the source. Thus the relative contributions of buoyancy and pressure gradient to the total vertical force F vary appreciably as air moves in across the perimeter of the source and up into the fire plume. The downward flow of neutral air outside the fire perimeter is driven predominantly by the pressure gradient, with a maximum upward effect of buoyancy inside the perimeter and weak upward buoyancy locally assisting an upward driving pressure gradient above the inner regions of the source.

At intermediate heights in the fire plume the horizontal (lateral) pressure gradients are very small (though the lateral pressure-gradient contribution in balance with the mean lateral turbulent transport of lateral momentum is neglected in this model as in most fire-plume models), and the vertical force is predominantly due to buoyancy calculated, rather more appropriately in this case, relative to the air temperature outside the fire plume (approximately T_0). Figure 3 (*a*) shows for experiment 1 the separate vertical profiles above the centre

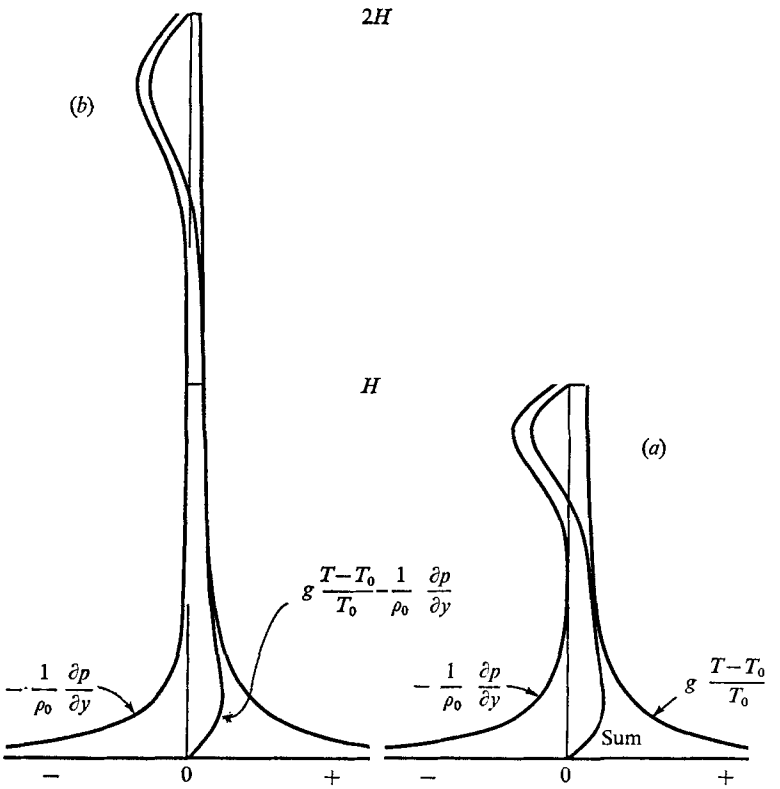

FIGURE 3. Comparison of vertical profiles on the symmetry axis $x = 0$ of a buoyancy force $g(T-T_0)/T_0$ and a vertical pressure-gradient force $-\rho_0^{-1}\partial p/\partial y$, calculated relative to the initial hydrostatic fields T_0 and p_0, with the total vertical force $F = g(T-T_0)/T_0-\rho_0^{-1}\partial p/\partial y$. Close above the source the large 'buoyancy' force is almost in balance with a hydrostatic pressure field, neither of which have any great significance, but the total force F is significant.

of the source ($x = 0$) of 'buoyancy calculated relative to T_0' and 'vertical dynamic pressure gradient calculated relative to hydrostatic equilibrium at T_0', together with the net profile of vertical force F. Although some help in understanding fire behaviour can be obtained from the 'buoyancy' and 'pressure-gradient' profiles separately, the F profile provides most of the information. In this case there is only a shallow central region above the immediate neighbourhood of the fire in which pressure gradients are small and the plume is driven predominantly by buoyancy according to the assumptions of entrainment models for turbulent jets or plumes. Above this is an upper region of large positive vertical pressure gradient and net negative F associated with a large negative horizontal pressure gradient; this is a region of strong vertical deceleration and large horizontal acceleration of air from the fire plume into an outward stream flowing under the inversion. Figure 3 (*b*) shows an equivalent set of profiles above the source centre for a case identical with experiment 1 except that both H and L have been doubled without changing the grid spacing or l. A comparison of the lower regions of figures 3 (*a*) and (*b*) in which the fire plume is generated and the upper regions

in which it is diverted into a venting outflow shows scarcely any change, but the central region in which the behaviour of the fire plume approaches that assumed in entrainment models has increased dramatically in vertical extent. Thus in figure 3 (*b*) ($H/l = \frac{96}{9}$) the pressure gradients are quite small and an entrainment model would be acceptable in a central region extending through perhaps two-thirds of the total height H. However, even in the weakly heated system of our model it is clear that plume theories cannot be applied near the source, where the pressure-gradient forces are comparable with the buoyancy forces (or, again, near the inversion). Thus previous attempts to model fixed fires using the various entrainment models developed for unrestricted plumes have very limited relevance to flow behaviour in the lowest part of fire columns, where almost all the combustion takes place. Fire wind, which is clearly driven by pressure-gradient forces, must play the dominant role in introducing oxygen for combustion and is absent from the earlier plume entrainment models. These facts may in part account for the difficulties in satisfying the 'fire link' constraint in liquid-pool fire models that have been described by Smith (1969) and Blest (1973), though the combustion zone in a liquid-pool fire may be of considerably greater vertical extent than that of wood-fuel fires.

The horizontal gradient of dynamic pressure and vertical component of force F are generally small elsewhere in the flow field, though there is a tendency in some calculations for increased values especially near the outer corners $(L, 0)$ and (L, H) of the computational region. These are caused by constraints imposed on the flow by our selection of lateral boundary conditions and provide a measure of our success in securing open-boundary flow. In the experiment illustrated our choice of horizontal motion ($v = 0$) across the lateral boundary appears to provide a reasonably satisfactory approximation at these Rayleigh numbers, but in other cases and especially at lower Ra values corner regions of pressure gradient are needed to adjust the streamline inclinations. Stable stratification also tends to produce horizontal flow with reduced disturbance to the pressure field.

It seems reasonable to assume that the flow realization of our numerical experiment 1 yields useful information about what happens in the admittedly much more complicated case of a fire. The weakness of the pressure-gradient/force field everywhere except possibly in the corners of the computational region indicates that there is very little dynamic pressure coupling between flow near the lateral boundary and the fire plume, and almost as little between the venting outflow under the inversion and the zone of fire wind and strong buoyant acceleration immediately above the source. Thus at large Rayleigh numbers, when the outer flow is dominated by advection rather than diffusion, there should be little back-coupling between flow near the source and either the venting outflow or the effects of the nearby lateral boundary. Moreover, it may be seen from figure 2 (*a*) that the lateral inflow near the edge of the fire has the character of flow towards a sink rather than that of an inflowing boundary layer; this may be expected to reduce the control of vertical diffusion over the inward mass flux, and thereby limits errors due to the modelling of diffusion that might otherwise affect our estimate of the inflow which would in a real fire support the combustion. For these reasons we expect that the solutions presented in figures 2 (*a*)–(*d*) will give

a reasonable simulation of buoyantly accelerated motion above a fixed heat source in a rigid horizontal boundary, and will therefore incorporate the principal dynamical effects arising in the neighbourhood of a fixed fire, including the inflow over the fire perimeter.

One obvious limitation of our model in relation to fire-induced air flow lies in our use of constant eddy diffusivities. Over a real fire we must expect large variations in turbulent intensity and hence in diffusivity between the various flow regions, including the convection column above the source where the density stratification is unstable, the sink-like lateral inflow of only weakly sheared air at uniform temperature and the stably stratified venting outflow. However, although we may have grossly overestimated diffusion in the outflow and underestimated it in the fire plume, this does not appear to have affected unduly the flow near the fire, to judge from the pressure-gradient or temperature fields. Moreover, the selection of a thermally insulating free-slip upper boundary condition appears not to be a serious restriction on the model, since though in general there would be a non-zero flux of heat and momentum through an inversion resulting in progressive erosion with possible local changes in height, the typical time scales for significant inversion changes are of the order of hours whereas fixed fires of this kind seldom burn as long as an hour at high intensity.

Our numerical experiment has at no stage been intended to model a fire directly, but it seems likely that our solutions may nevertheless yield insight into a number of aspects of fire-induced air flows. Thus the width of the fire plume, which may be judged most readily from the isotherm pattern as in figure 2 (*c*), appears to be geometrically constrained by the width of the source and changes little further in width with changing Rayleigh number once the pseudo-Rayleigh number is sufficiently large. We recall that the spread angle of a turbulent jet or plume is independent of the Reynolds (Rayleigh) number, provided that this is large enough for fully developed turbulent flow. Thus in our fire simulation an advective/diffusive balance is apparently achieved within the fire plume as the Rayleigh number is increased, but the outer flow becomes increasingly advective. Again, the fire wind is like a sink flow towards a sink within the heat source, and although there will undoubtedly be some effect of ground roughness in the outer ground boundary layer, this should not exercise a significant control over mass inflow and hence over combustion rates.

Up to this stage our results have been discussed in terms of a single realization (with $Ra = 2600$, $H/L = 1$, and $T = 300\,^{\circ}\mathrm{K}$ in the inflow and $T_x = 0$ in the outflow at the lateral boundary $x = L$). It remains for us to demonstrate that these results are not unduly and inappropriately influenced by the choice of parameter values, lateral boundary conditions or computational region. The dependence of the overall flow on this choice of conditions raises issues which may be relevant in the numerical simulation of other mesoscale geophysical flows. To keep the present paper within reasonable bounds we shall discuss these wider implications in a separate paper, and here restrict ourselves to a limited range of comparisons to show that the solution near the source is insensitive to the exact choice of conditions provided that these are suitably selected.

The streamline patterns are broadly similar in all our numerical experiments,

especially near the source, where sink-like inflow and upward deflexion of the air stream into the fire plume are dominant features. However, one aspect of flow that does not appear in figure 2 (*a*) is the tendency in some cases for the development of a weak region of closed streamlines outside the main fire plume and at middle heights. This tendency is more pronounced at smaller aspect ratios H/L (at fixed H/l) and with the boundary condition $T_x(L, y) = 0$ $(y < h)$ rather than $T(L, y) = T_0$ $(y < h)$, but it decreases as the pseudo-Rayleigh number increases. The tendency to form standing eddies of this kind appears to be related to restrictions on the freedom of lateral flow, and may result from stable ambient stratification or possibly from topography. Such eddies combine with the sink-like inflow at lower levels to reinforce the downward and inward nature of flow into the 'fire', although the effect is relatively weak in the cases we have computed. This is the only indication in any of our numerical experiments that might be related to the downward and inward flowing jets of air reported by Palmer (1969, private communication) from a series of experiments on large fires near Montgomery Pass, Nevada.

The effects of parameter values, lateral boundary conditions and computational box size on the solutions are shown very clearly in the temperature fields, and these form the basis for the remaining discussion.

Figures 4 (*a*) and (*b*) show a comparison of isotherm patterns with our two different thermal boundary conditions on the lateral inflow for pseudo-Rayleigh numbers of 2600 and 72 respectively. At the lower Rayleigh number there is a considerable difference between the two solutions; with the condition $T(L, y) = T_0$ $(y < h)$ there is an extensive wedge of inflowing cold air at or near the ambient temperature T_0, whereas with the condition $T_x(L, y) = 0$ the inflowing air is stably stratified with a roughly uniform vertical temperature gradient. The latter solution requires an appreciably longer computation time to reach equilibrium, and in spite of the fact that both were computed for a Rayleigh number $Ra = 72$ the details of the inflow might be regarded as convectively controlled when the inflow temperature is specified and diffusively controlled when a zero temperature gradient is specified. This difference arises in part because we have selected a computational region of fixed width for a flow which in principle must continue to develop outside our region and in part because of the two-dimensional nature of our problem. We shall discuss this question in more detail elsewhere, but for our present discussion of fire wind it is sufficient to note that *for this problem* at relatively low pseudo-Rayleigh numbers the lateral condition $T = T_0$ on the inflowing air provides better modelling for a fire in an extensive environment. At relatively high Rayleigh numbers, however, there is little difference between the solution fields as the outer flow is dominated by advective heat transfer in any case. Large fires correspond to high Rayleigh numbers and we are then free to choose either of the lateral thermal boundary conditions; where there is such a choice, we prefer the condition $T(L, y) = T_0$ $(0 < y < h)$.

The dependence of solutions on the aspect ratio H/L of the computational region is also shown clearly by a comparison of isotherm patterns. Figure 5 (*a*) shows a comparison of the isotherms for experiments 5 and 7, at a Rayleigh number 650 and with $T(L, y) = T_0$ in $0 \leqslant y < h$; the isotherms for experiment 5,

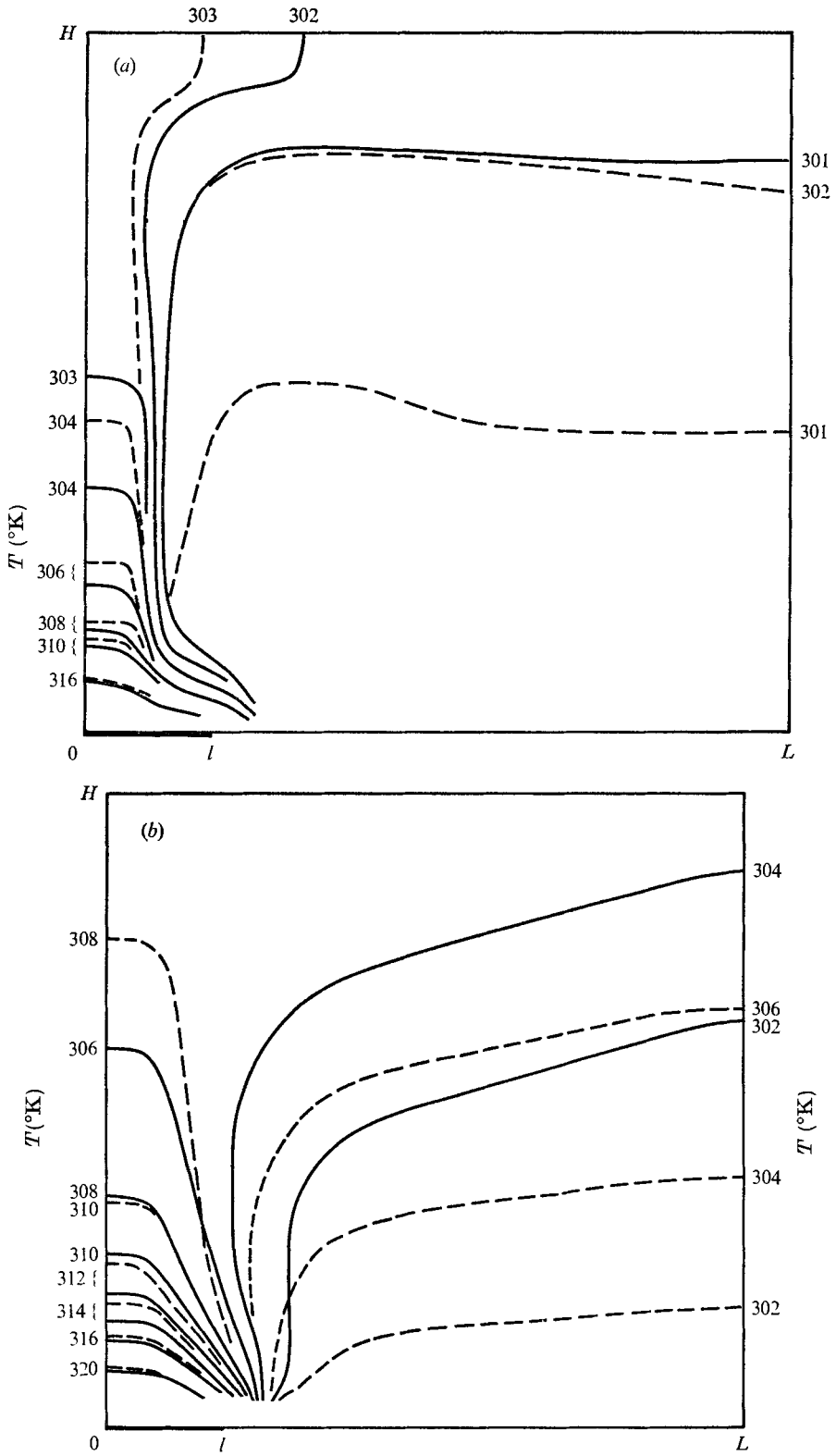

FIGURE 4. A comparison of the temperature fields for the alternative thermal conditions $T = T_0$ (solid lines) and $T_x = 0$ (broken lines) on the portion $0 \leqslant y < h$ of the lateral boundary $x = L$ in the cases (*a*) $Ra = 2600$ and (*b*) $Ra = 72$. In each case the aspect ratios H/L and H/l are held fixed with values 1 and $\frac{4}{9}\frac{8}{9}$ respectively. (See text for discussion.)

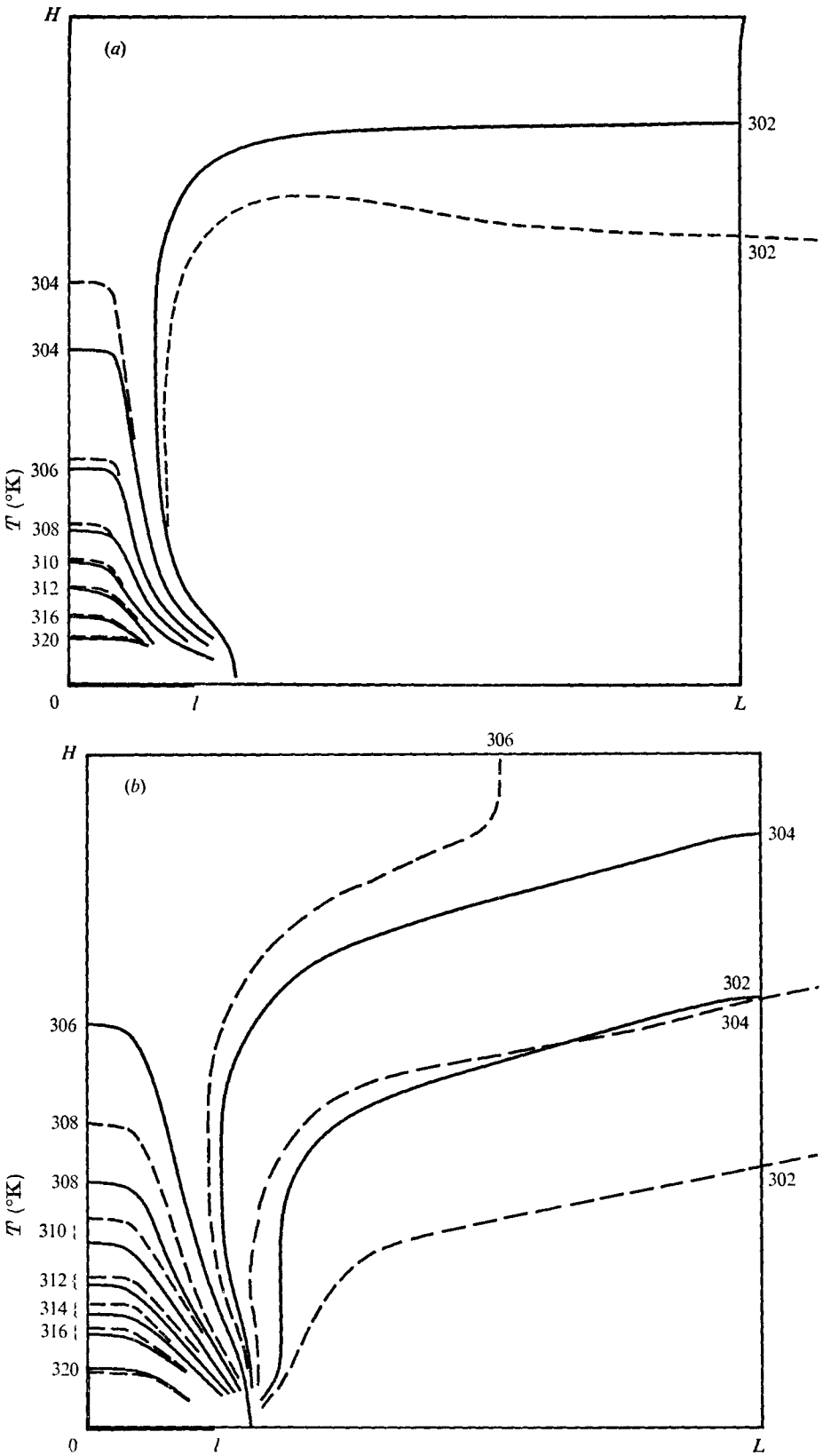

FIGURE 5. A comparison of the temperature fields for two values of the aspect ratio $H/L = 1$ (solid lines) and $\frac{1}{2}$ (broken lines) in the cases (*a*) $Ra = 650$ and (*b*) $Ra = 72$. In each case the thermal condition on the portion $0 \leqslant y < h$ of the lateral boundary $x = L$ is taken as $T = T_0$, and the aspect ratio H/l is held fixed equal to $\frac{4.8}{9}$.

with $H/L = 1$, are shown by continuous curves and the inner part ($x < L$) of those for experiment 7, with $H/L = \frac{1}{2}$, by broken curves. Figure 5 (*b*) shows a similar comparison at a Rayleigh number of 72 of experiment 9, with $H/L = 1$ (continuous curves), and experiment 11, with $H/L = \frac{1}{2}$ (broken curves). We prepared also isotherms for experiments 6 and 8, at a Rayleigh number of 650, but with the alternative lateral boundary condition $T_x(L, y) = 0$ ($0 \leqslant y < h$), to establish the effect of varying the aspect ratio H/L. However, the difference was not appreciably greater than with the alternative lateral thermal condition (see figure 5*a*) and there is no point in reproducing them here. Thus, it may be seen that at the smaller values of the pseudo-Rayleigh number there is a significant effect on the temperature field near the heat source due to the size of computational region and considerable care should be taken in selection of lateral boundary conditions and computational region. At $Ra = 2600$, however, the temperature fields show so little difference in the neighbourhood of the fire that we can reasonably claim that the inner flow and temperature fields are independent of the box size and of the outer boundary, and we believe that our solution fields are representative of convection over a heat source at these larger pseudo-Rayleigh numbers.

REFERENCES

Arakawa, A. 1966 Computational design for long term numerical integration of the equations of fluid motion, part 1. *J. Comp. Phys.* **1**, 119–143.

Blest, D. C. 1973 Ph.D. thesis, Monash University.

Lee, S. L. & Emmons, H. W. 1961 A study of natural convection above a line fire. *J. Fluid Mech.* **11**, 353–358.

Lilly, D. K. 1964 Numerical solutions for the shape-preserving two-dimensional thermal convection element. *J. Atmos. Sci.* **21**, 83.

Morton, B. R. 1965 Modelling fire plumes. 10*th Symp.* (*Intn.*) *on Combustion, Combustion Inst., Pittsburgh*, pp. 973–982.

Morton, B. R. 1967 On the dynamics of fire plume convection. *Proc. Mass Fire Res. Symp., Washington, DASIAC Special Rep.* no. 59, p. 84.

Murgai, M. P. & Emmons, H. W. 1960 Natural convection above fires. *J. Fluid Mech.* **8**, 611–624.

Nielson, H. J. & Tao, L. N. 1965 The fire plume above a large free-burning fire. 10*th Symp.* (*Intn.*) *on Combustion, Combustion Inst., Pittsburgh*, pp. 965–972.

Platzman, G. W. 1963 The dynamic prediction of wind tides on Lake Erie. *Meteor. Monog.* **4**, 44.

Quon, C. 1972 High Rayleigh number convection in an enclosure – a numerical study. *Phys. Fluids*, **15**, 12.

Smith, R. K. 1969 The constraints on the airflow above fires. *Proc. TCP Mass Fire Symp., Canberra, Australia, Paper*, B 3. (See also *G.F.D. Lab., Monash University, Paper*, no. 18.)

Steward, F. R. 1970 Prediction of the height of turbulent diffusion buoyant flames. *Comb. Sci. T.* **2**, 203–212.

Williams, G. P. 1967 Thermal convection in a rotating fluid annulus – part 1. *J. Atmos. Sci.* **24**, 144–161.